Research Article Vol. 12, No. 11 / 1 Nov 2022 / Optical Materials Express 4435

Optical Materials EXPRESS

High precision reconstruction for compressed femtosecond dynamics images based on the TVAL3 algorithm

FEI YIN,[1,2,4] YIZHAO MENG,[3,4] QING YANG,[1,5] LIN KAI,[3] YI LIU,[3] XUN HOU,[3] YU LU,[3,6] AND FENG CHEN[3,*]

[1] *School of Mechanical Engineering, Xi'an Jiaotong University, Xi'an, 710049, China*
[2] *Key Laboratory of Ultrafast Photoelectric Diagnostics Technology, Xi'an Institute of Optics and Precision Mechanics (XIOPM), Chinese Academy of Sciences (CAS), Xi'an, Shaanxi 710119, China*
[3] *State Key Laboratory for Manufacturing System Engineering and Shaanxi Key Laboratory of Photonics Technology for Information, School of Electronic Science and Engineering, Xi'an Jiaotong University, Xi'an, 710049, China*
[4] *These authors contributed equally to this work*
[5] *yangqing@mail.xjtu.edu.cn*
[6] *luyu90@xjtu.edu.cn*
[*] *chenfeng@mail.xjtu.edu.cn*

Abstract: Compressed sensing (CS) has been successfully demonstrated to reconstruct ultrafast dynamic scenes in ultrafast imaging techniques with large sequence depth. Since compressed ultrafast imaging used a two-step iterative shrinkage/thresholding (TwIST) algorithm in previous image reconstruction, some details of the object will not be recovered when the amount of data compression is large. Here we applied a more efficient Total Variation (TV) minimization scheme based on augmented Lagrangian and alternating direction algorithms (TVAL3) to reconstruct the ultrafast process. In order to verify the effectiveness of the TVAL3 algorithm, we experimentally compare the reconstruction quality of TVAL3 algorithm and TwIST algorithm in an ultrafast imaging system based on compressed-sensing and spectral-temporal coupling active detection with highest frame rate of 4.37 trillion Hz. Both dynamic and static experimental results show that, TVAL3 algorithm can not only reconstruct a rapidly moving light pulse with a more precise profile and more fitted trajectory, but also improve the quality of static objects and the speed of reconstruction. This work will advance the ultrafast imaging techniques based on compressed sensing in terms of image reconstruction quality and reconstruction speed, which finally helps promoting the application of these techniques in areas where high spatial precision is required, such as phase transitions and laser filamentation in nonlinear solids, etc.

1. Introduction

Nowadays, researchers have discovered various phenomena with great scientific significance. These phenomena usually happen in very short time scales. For example, the investigation about laser-material interactions, especially about optical material modification [1–3] and laser filamentation [4] are critical to the development of advanced optical waveguide, photonics crystals, and ultrashot pulse laser. But these processes are in the picosecond domain. Moreover, the study of molecular dynamics, which happens in the femtosecond domain can provide experimental basis for the study and control of chemical reactions, molecular phase transitions, etc. To reveal the essence of these microscopic processes, ultrafast photography and measurement technologies with extremely high imaging speed have been proved to be a powerful tool [5]. Pump-probe technique can detect ultrafast processes that happens in femtosecond scale [6,7]. However, it cannot observe events that are difficult-to-reproduce or non-repetitive. Recently, several techniques have also

#468475 https://doi.org/10.1364/OME.468475
Journal © 2022 Received 29 Jun 2022; revised 30 Sep 2022; accepted 13 Oct 2022; published 21 Oct 2022

Optical Materials EXPRESS

emerged to obtain multiple images of ultrafast processes with a single detection, such as angle-division-based multiple-camera (ADMC) [8], multiframe femtosecond time-resolved optical polarography (M-FTOP) [9], sequentially timed all-optical mapping photography (STAMP) [10,11]and frequency recognition algorithm for multiple exposures (FRAME) [12]. Among these promising methods, although they can record ultrafast processes with extremely high temporal resolution, the sequence depth is limited. To get enough frames, the amount of data increases. In this way, there will be difficulties in the storage, transmission and recovery of information. To address this challenge, many ultrafast imaging systems utilize compressed sensing (CS) algorithms [13] to reconstruct high-dimensional data from acquired low-dimensional data.

For the ultrafast imaging techniques based on CS algorithms [14–17], the temporal slices of an ultrafast scene are spatially encoded and compressed into a single 2D image. In previous work, most of the ultrafast image sequences were reconstructed from the compressed 2D image using a two-step iterative shrinkage/thresholding (TwIST) algorithm [18]. The two steps in the TwIST algorithm can be considered as iterative convergence and denoising [19]. So far, TV (Total Variation) minimization has been used as the denoising step of TwIST in compressed ultrafast imaging. The first few iterations of the TwIST algorithm could give satisfactory reconstruction results, but the remaining iterations may be sometimes not. Due to the functional characteristics of the TV model itself, with the frame further increases, it still lacks a certain robustness when reconstructing images. Moreover, the main time-consuming part of running TwIST is the denoising step operation. Considering that many important ultrafast processes happen in the field of microscopy, which means that to have a clear knowledge about them need a spatial measurement with high precision reconstruction, the current reconstruction quality in compressed ultrafast imaging should be improved. In this paper, we applied a more efficient TV minimization scheme based on augmented Lagrangian and alternating direction algorithms (TVAL3) to reconstruct the ultrafast process in femtosecond scale [20,21]. TVAL3 algorithm was applied by Yang et al. [22] in a compressed imaging system based on streak camera for passive-detecting. Due to the electron optical structure in the streak camera, additional aberrations, such as distortion, astigmatism, will be introduced, resulting in limited image quality. Here, we use an all-optical active-detecting system named compressed ultrafast spectral-temporal photography [15], which can achieve higher imaging quality. Compressed ultrafast spectral-temporal photography is capably of measuring the transient events at speeds up to 10^{12} frames per second (fps) with a sequence depth of tens of frames in a single shot. Moreover, it can also recover the spectral imaging with sub-nm resolution. We experimentally measured a detective laser illuminating the static objects and light propagations with highest frame rate of 4.37 trillion Hz. From the static and femtosecond dynamic reconstruction results, the reconstruction performance of TVAL3 algorithm shows great progress in spatial resolution and accuracy of reconstruction of unknown ultrafast processes compared with TwIST algorithm.

2. Principle and experiment

In the experiment, a *fs* pulse is stretched to chirped pulse by grating group of optical dispersion elements. In the chirped pulse, the frequency of pulse changes with time. In this way, according to spectral-temporal coupling, different wavelength corresponds to different time. When an ultrafast dynamic scene $\boldsymbol{O}(\boldsymbol{x},\boldsymbol{y},\boldsymbol{t})$ is detected by the stretched pulse, different temporal segments of $\boldsymbol{O}(\boldsymbol{x},\boldsymbol{y},\boldsymbol{t})$ are detected by different spectral components and converted into spectral-temporal image sequence. The spatial-temporal distribution of the stretched pulse is denoted as a density matrix $\boldsymbol{I}(\boldsymbol{x},\boldsymbol{y},\boldsymbol{t})$ or $\boldsymbol{I}(\boldsymbol{x},\boldsymbol{y},\boldsymbol{\lambda})$. Then the coded aperture spatially encodes the spectral-temporal image sequence with a pseudorandom binary pattern, which can be donated as matrix, $\mathbf{C}$. The encoded scene is spatially dispersed by a dispersive element, and then the 3D *x*-*y*-*t* date cube is transformed into a 2D image to be recorded by CCD, the process of which is donated by matrix, $\boldsymbol{T}$. $\mathbf{C}$ and $\boldsymbol{T}$ are used to record images according to the CS theory. Only the images processed in

Optical Materials EXPRESS

this way can be restored by the CS algorithm [23]. In this paper, our reconstruction processes are all done using MATLAB R2020b on a computer configured with Intel(R) Core (TM) I7-10700 CPU @ 2.90GHz. The 2D image $\mathbf{E}(\boldsymbol{x},\boldsymbol{y})$ can be written as

$$\boldsymbol{E}(x,y) = \boldsymbol{T}\cdot\boldsymbol{C}\cdot\boldsymbol{I}\cdot\boldsymbol{O}\cdot(x\cdot y\cdot t) = \phi\cdot\boldsymbol{O}(x,y,z) \tag{1}$$

Where $\boldsymbol{T}$ is an image compressor, $\boldsymbol{C}$ is a spectral-temporal encoder, $\boldsymbol{I}$ is a density matrix, and we define $\emptyset = \boldsymbol{T}\cdot\boldsymbol{C}\cdot\boldsymbol{I}$, $\emptyset$ is a transform matrix. A clearer mechanism representation is shown in Fig. 1(a). In Eq. (1), the data cube of observation images $\boldsymbol{E}$ is much smaller than that of the ultrafast target $\boldsymbol{O}(\boldsymbol{x},\boldsymbol{y},\boldsymbol{t})$, so it is an ill-conditioned problem to solve. According to the compressed sensing theory, the $\boldsymbol{O}(\boldsymbol{x},\boldsymbol{y},\boldsymbol{t})$ we need can be acquired by solving an optimization problem:

$$min_{\boldsymbol{O}(\boldsymbol{x},\boldsymbol{y},\boldsymbol{t})}\sum_i \| D_i\boldsymbol{O} \|,\ \text{s.t. } \phi\boldsymbol{O} = \boldsymbol{E} \tag{2}$$

Where $D_i\boldsymbol{O}$ is a discrete gradient calculation for each pixel of $\boldsymbol{O}(\boldsymbol{x},\boldsymbol{y},\boldsymbol{t})$ horizontally and vertically.

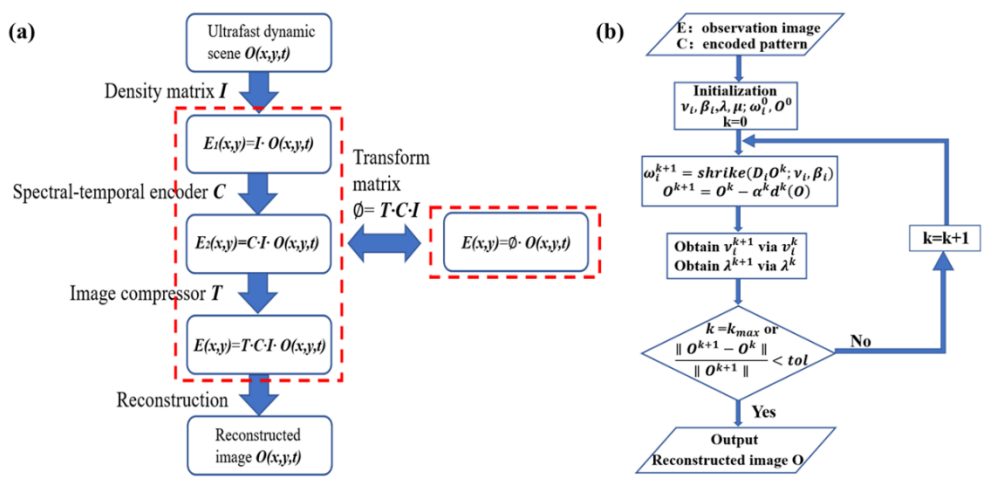

Fig. 1. (a) Schematic diagram of ultrafast imaging techniques based on CS algorithms; (b) Flow chart of the TVAL3 algorithm

Furthermore, Eq. (2) has been proved to be equivalent to Lagrangian function, which is expressed as:

$$\min_{\boldsymbol{O}(\boldsymbol{x},\boldsymbol{y},\boldsymbol{t})} \mathcal{L} = \sum_i \| D_i\boldsymbol{O} \| - \lambda(\boldsymbol{E} - \phi\boldsymbol{O}) \tag{3}$$

In order to solve the above equations, researchers have applied the TwIST algorithm to the TV model to solve the fast optimization problem in recent years. The problem solved by the TwIST algorithm can be expressed as follows:

$$\hat{\boldsymbol{O}} = \arg\min_{\boldsymbol{o}} \left\{ \frac{1}{2} \| \boldsymbol{E} - \phi\boldsymbol{O} \|_2^2 + \lambda \left(\sum_i \| D_i\boldsymbol{O} \| \right) \right\} \tag{4}$$

Where $\sum_i \| D_i\boldsymbol{O} \|$ is called the regularizer which usually is total variation (TV), λ is the regularization parameter that balances the fidelity term $\|\boldsymbol{E} - \emptyset\boldsymbol{O}\|_2^2$ and the regularizer $\sum_i \| D_i\boldsymbol{O} \|$. Since the main time-consuming part of the TwIST algorithm is the TV noise reduction part, this makes the algorithm's time to calculate the reconstruction results much slower than that of the l_1 solver. Also, due to the non-differentiability and nonlinearity of the TV model, the Eq. (2) is difficult to solve. In previous research, Wang, Yang, Yin et al. applied the alternating

Optical Materials EXPRESS

minimization method to the TV model to deconvolute and denoise the image. Although the solution speed of this method is much faster than that of the l_1 solver, the available measurement matrices are limited.

Based on the idea of solving the TV model by this alternating minimization method, this part will introduce the TVAL3 algorithm. TVAL3 combines the augmented Lagrangian (AL) function method and the alternating minimization method on the basis of the TV algorithm, and then uses the steepest descent method to find the minimum value and improve the signal-to-noise ratio of the image.AL function is written as:

$$\min_{\omega_i,\boldsymbol{O}} \sum_i \parallel \omega_i \parallel, \text{s.t.} \phi\boldsymbol{O} = \boldsymbol{E} \text{ and } \boldsymbol{D_i O} = \boldsymbol{\omega_i} \text{ for all } i \tag{5}$$

By compare Eq. (2) and Eq. (5), since the term $\|\cdot\|$ in the TV model is non-differentiable, we introduce a slack variable ω_i at each pixel to move the non-differentiable term out. The augmented Lagrangian function corresponding to Eq. (5) is:

$$\begin{aligned}\min_{\omega_i,\boldsymbol{O}} \mathcal{L}(\omega_i, \boldsymbol{O}) = \sum\nolimits_i (\parallel \omega_i \parallel - v_i^T (D_i\boldsymbol{O} - \omega_i) + \frac{\beta_i}{2} \parallel D_i\boldsymbol{O} - \omega_i \parallel_2^2) \\ - \lambda^T (\boldsymbol{E} - \phi\boldsymbol{O}) + \frac{\mu}{2} \parallel \boldsymbol{E} - \phi\boldsymbol{O} \parallel_2^2\end{aligned} \tag{6}$$

In order to facilitate the solution of the above equation and overcome the non-differentiability and nonlinearity mentioned above, TVAL3 uses the alternating minimization method at each iteration to solve. The above formula is divided into two sub-formulas, the first formula is "ω-subproblem":

$$\min_{\omega_i} \sum\nolimits_i (\|\omega_i \parallel - v_i^T (D_i\boldsymbol{O}^{(\boldsymbol{k})} - \omega_i) + \frac{\beta_i}{2} \parallel D_i\boldsymbol{O}^{(\boldsymbol{k})} - \omega_i \parallel_2^2) \tag{7}$$

The result of Eq. (7) is as follow:

$$\begin{aligned}\omega_i^{(\boldsymbol{k}+1)} &= max\left\{\left|D_i\boldsymbol{O}^{(\boldsymbol{k})} - \frac{v_i}{\beta_i}\right| - \frac{1}{\beta_i}, 0\right\} sgn\left(D_i\boldsymbol{O}^{(\boldsymbol{k})} - \frac{v_i}{\beta_i}\right) \\ &= shrike\left(D_i\boldsymbol{O}^{(\boldsymbol{k})}; v_i, \beta_i\right)\end{aligned} \tag{8}$$

Then, use the solved $\omega_i^{(k+1)}$ to solve the second formula is "$\boldsymbol{O}^{(\boldsymbol{k}+1)}$-subproblem":

$$\begin{aligned}\min_{\boldsymbol{O}} \mathbb{Q}^{\boldsymbol{k}}(\boldsymbol{O}) * = \sum\nolimits_i (-v_i^T (D_i\boldsymbol{O} - \omega_i) + \frac{\beta_i}{2} \parallel D_i\boldsymbol{O} - \omega_i \parallel_2^2) \\ - \lambda^T (\boldsymbol{E} - \phi\boldsymbol{O}) + \frac{\mu}{2} \parallel \boldsymbol{E} - \phi\boldsymbol{O} \parallel_2^2\end{aligned} \tag{9}$$

The gradient of $\mathbb{Q}^k(\boldsymbol{O})$ is

$$d^{\boldsymbol{k}}(\boldsymbol{O}) = \sum_i (\beta_i D_i^T (-D_i\boldsymbol{O} - \omega_i^{(\boldsymbol{k}+1)}) - D_i^T v_i) + \mu\phi^T(\boldsymbol{E} - \phi\boldsymbol{O}) - \phi^T \tag{10}$$

Steepest descent method can update $\boldsymbol{O}^{(\boldsymbol{k}+1)}$:

$$\boldsymbol{O}^{(\boldsymbol{k}+1)} = \boldsymbol{O}^{(\boldsymbol{k})} - \alpha^{\boldsymbol{k}} d^{\boldsymbol{k}}(\boldsymbol{O}) \tag{11}$$

α is compute step length. The parameters v_i and λ are updated as follows:

$$v_i^{\boldsymbol{k}+1} = v_i^{\boldsymbol{k}} - \beta_i^{\boldsymbol{k}} (D_i\boldsymbol{O}^{(\boldsymbol{k}+1)} - \omega_i^{\boldsymbol{k}+1}) \tag{12}$$

$$\lambda^{\boldsymbol{k}+1} = \lambda^{\boldsymbol{k}} - \mu^{\boldsymbol{k}} (\boldsymbol{E} - \phi\boldsymbol{O}^{\boldsymbol{k}+1}) \tag{13}$$

So far, both the ω-subproblem and the $\boldsymbol{O}$-subproblem are solved. By using the above iterative formula, the optimal solution of the original signal can be found. For a clearer representation, the algorithm flow chart is shown in Fig. 1(b).

Optical Materials EXPRESS

3. Result and discussion

3.1. Reconstructions of static spectral images

In order to prove the superiority of TVAL3 algorithm, we firstly performed acquisition reconstruction of the resolution test chart in this system. The experimental setup is shown in the Fig. 2(a). At first, a designated spectrum of the fs pulse transmits through the resolution test chart. After that, the wavefront carries the information of the object which is imaged via a 4f imaging system (Both lenses have a focal length of 200mm) on a transmission mask. Then the mask encodes the image which carries the spectral information. The encoded spectral image is spatially modulated by the dispersion grating, different wavelengths correspond to different spatial positions during this process [24]. Finally, the wavelength-dependent images are intensity-superimposed on the CCD plane and recorded by the 2D CCD, as shown in the Fig. 2(b). In this system, we collected and reconstructed 50 frames of the element of the resolution test chart. The spectral resolution is 0.25nm. The spatial resolution is 2.83lp/mm. Since the dispersion grating disperses the spectral image in the lateral direction, the vertical lines in the 4 element will overlap each other so that a large part of the information will be overwritten. Figure 2(c) shows the reconstruction images by the TwIST and TVAL3 algorithms, respectively. In order to compare the reconstruction quality of the two algorithms more clearly, we plot the intensity curve of the reconstructed image at the blue line, as shown in the right panel of Fig. 2(c). Compared with the intensity curve of the static image (Fig. 2(d)), the TVAL3 algorithm reconstructs the vertical lines with a higher contrast, and all the vertical lines are reconstructed clearly and distinguishably in the displayed frames, while more background noise is involved for the recovery results of the TwIST algorithm.

What's more, in the case of different compression ratios, the reconstruction quality of the two algorithms is compared. The reconstruction results of the 13th frame (corresponds to 799.01nm) under different compression ratios are shown in Fig. 2(e) and (f). Figure 2(e) shows the phenomenon that as the number of acquisition frames increases, the reconstructed vertical lines becomes more and more blurred, while the reconstructed vertical lines of the TVAL3 algorithm have always been distinguishable. Figure 2(g) and (h) are the intensity curves (located at the same place as the blue line drawn at the Fig. 2(c)) of the reconstruction results of the TwIST and TVAL3 algorithms when the number of acquisition frames varies from 20 to 50 frames. As these two figures clearly showing, the intensity contrast of reconstructed vertical lines by TwIST algorithm goes from high to low. In other words, the reconstruction quality of the TwIST algorithm decreases with the decrease of the compression ratio. Compared with the TVAL3 algorithm, the reconstruction quality of the TVAL3 algorithm within 50 frames is close to the original static image. In addition, the reconstruction speed of the observation images with the frame number ranging from 20 frames to 50 frames under different algorithms is compared. As shown in Fig. 2(i), the running time of the TVAL3 algorithm (from 20 to 50 frames are 53s, 57s, 85s, 87s, 115s, 124s, 141s, respectively) is much shorter than that of the TwIST algorithm (from 20 to 50 frames are 96s, 124s, 166s, 197s, 216s, 271s, 307s, respectively). Meanwhile, ratio between running times of TwIST and TVAL3 algorithms is shown in the inset in Fig. 2(i). As can be seen from the inset, the reconstruction speed of the TVAL3 algorithm is about twice as fast as that of the TwIST algorithm. Therefore, the TVAL3 algorithm not only has better reconstruction quality, but also faster reconstruction speed.

3.2. Reconstructions of light propagation

The experimental arrangement is shown in the Fig. 3(a). A beam of pump pulse acts on the medium based on the Kerr effect, which leads to the heterogeneous change of the refractive index of the medium [9,25]. At the same time, a beam of a chirped pulse passes through the medium as a probe pulse. Around the place where the pump light acts, the probe light will be birefringent at the corresponding position due to the Kerr effect. Only the probe light in this area can be detected

Optical Materials EXPRESS

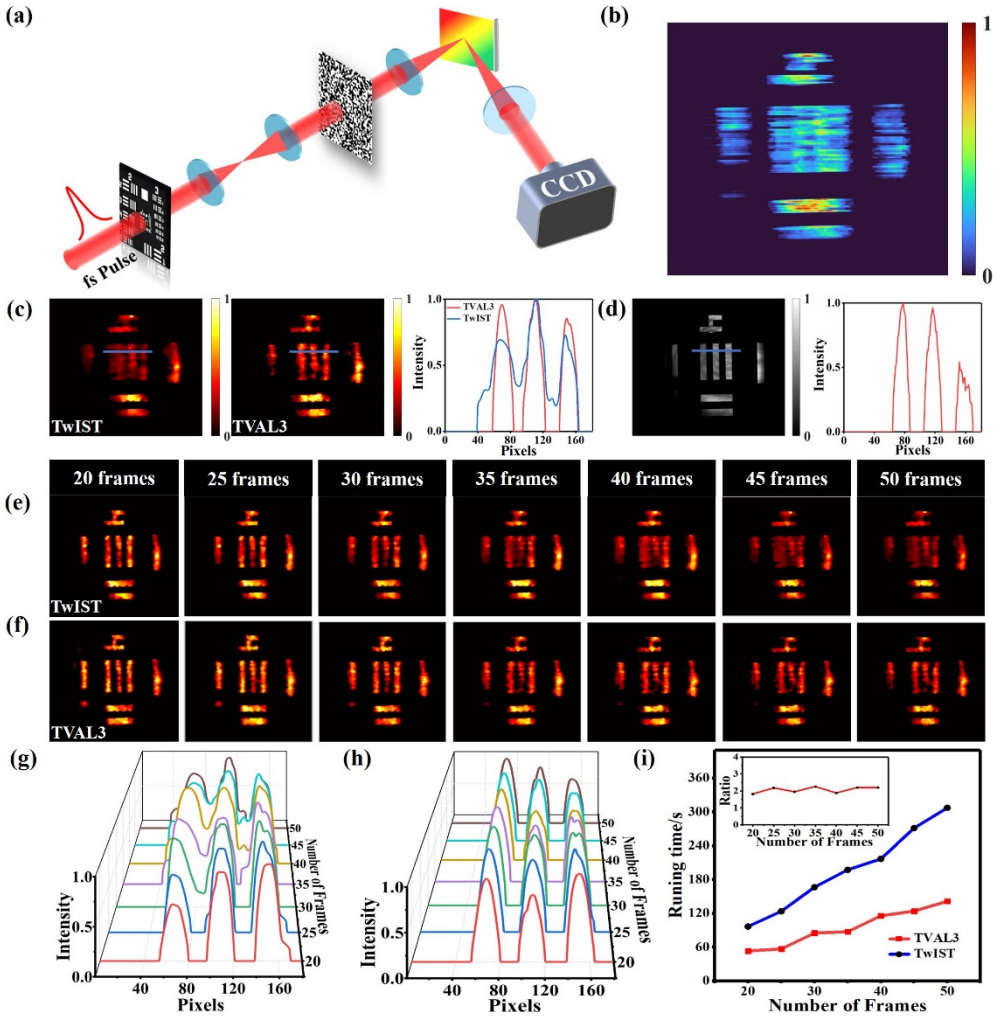

Fig. 2. Static experimental results. (a) Experimental setup for the spectral measurement of resolution test chart; (b) Observation image recorded by CCD; (c) Selected reconstructed image from TwIST and TVAL3 algorithms (left and middle) and intensity curve (right); (d) Recorded static image of test resolution target from external CCD (left) and intensity curve of the vertical lines (right); (e) and (f) Reconstructed results of the 13th frame under different compression ratios by TwIST and TVAL3 algorithms; (g) and (h) Intensity curves of the reconstruction results of the TwIST and TVAL3 algorithms from (e) and (f); (i) Running time of the TwIST and TVAL3 algorithms.

Optical Materials EXPRESS

by the subsequent system. Therefore, the probe pulse carries the information of light propagation. According to the principle of spectral-temporal coupling, the temporal information of the light propagation can be transferred into the spectral information and collected by the compressed camera. Figure 3(b) show the reconstructed images of three straight-propagating light pulses captured by this system under different algorithms (see Visualization 1, Visualization 2 and Visualization 3). The number of frames captured in each group is 30 frames. The frame interval in the three groups are 229fs, 384fs, and 337fs, which corresponds to the frame rate of 4.37, 2.6 and 2.97 trillion Hz respectively. The result of Fig. 3(b) shows one frame from six frames.

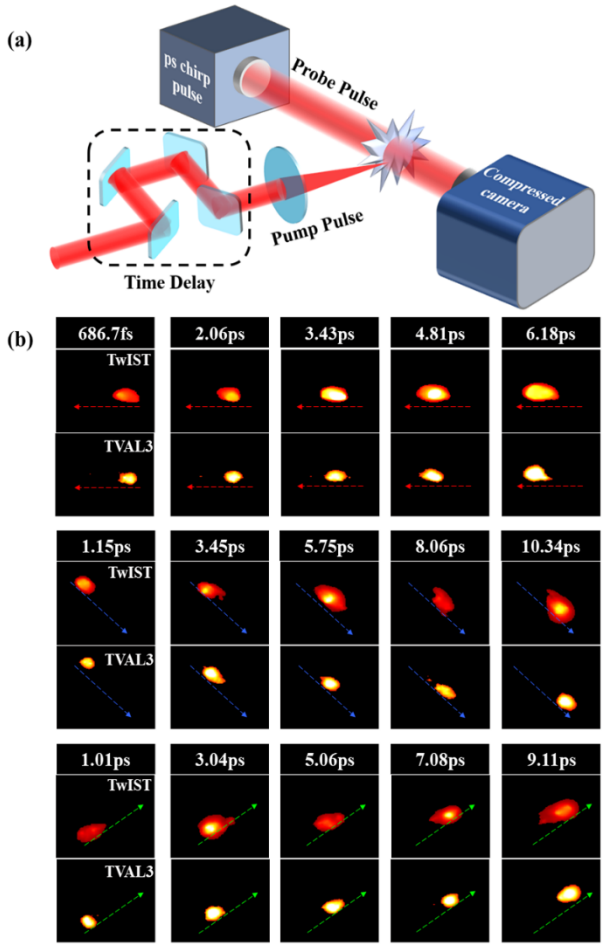

Fig. 3. Light propagation experimental results. (a) Experimental arrangement; (b) Three sets of reconstructed images of flying light pulse by TwIST and TVAL3 algorithms.

In order to have a clear comparison between the TwIST and the TVAL3 algorithms, we fitted the motion trajectory of the center of the light spot, as shown in Fig. 4(a) and (b). The straight lines of different colors in Fig. 4(a) and (b) correspond to the light spot trajectories marked by the corresponding colored arrows in Fig. 3(b). The center coordinates of the three groups of light spots reconstructed by the TVAL3 algorithm are basically on the fitted line, while the second group of light spots (blue line) reconstructed by the TwIST algorithm have many deviation points. What's more, the fit of the three groups of fitted curves are also calculated, as shown in Fig. 4(c). The fitting degree of three group of the reconstruction results of TwIST algorithm are 0.93, 0.94,

Optical Materials EXPRESS

0.85, respectively. However, these values in the reconstruction results of TVAL3 algorithm are 0.95, 0.99, 0.97, respectively. It is clearly shown that TVAL3 algorithm has a higher degree of fit, and they are all close to 1. So, the reconstruction results of TVAL3 have a better fit. In addition, computational imaging will always resolve some noise beyond the original signal. Therefore, the radial size of the reconstructed spot should be as close to the width of collected spot as possible. In other words, the smaller the width of the spot, the better the reconstruction effect. In order to compare the difference in the shape of the reconstructed light spots, we performed shape fitting on the first group of light spots reconstructed by the TwIST algorithm and the TVAL3 algorithm, as shown in Fig. 4(d). The reconstruction spot of the TwIST algorithm has 32 pixels on the long axis and 20 pixels on the short axis, while the reconstructed spot of the TVAL3 algorithm has 23 pixels on the long axis and 17 pixels on the short axis. In contrast, the light spot reconstructed by the TVAL3 algorithm should be closer to the original image. In addition, the length of the short axis has little difference with the width of the observed image of the collected light spot. Finally, conclusion can be got that the reconstruction quality of the TVAL3 algorithm is better than that of the TwIST algorithm.

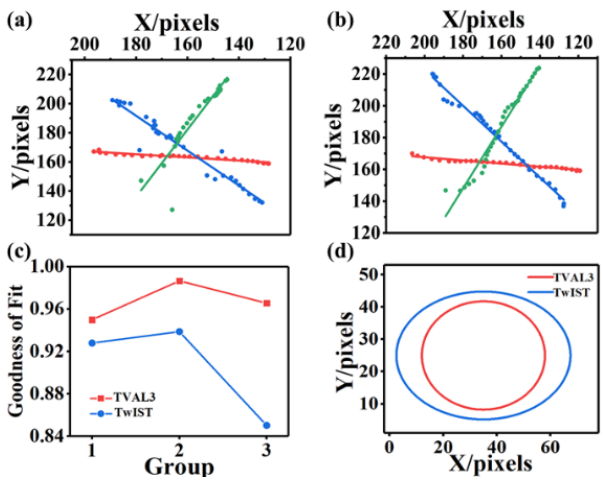

Fig. 4. Analysis of dynamic reconstruction results. (a) and (b) Fitted motion trajectory of light spot center of TwIST and TVAL3 algorithms, respectively; (c) The fit of the three groups of fitted curves; (d) Shapes of the reconstructed light spots

4. Conclusions

In conclusion, we successfully used the TVAL3 algorithm in the reconstruction process of the compressed ultrafast spectral temporal photography. Compared with the TwIST algorithm which is commonly used in the ultrafast imaging techniques based on CS algorithms, TVAL3 algorithm combines the augmented Lagrangian function method and the alternating minimization method on the basis of the original TV model, and then uses the steepest descent method to solve the inverse problem. We have experimentally proved that the TVAL3 algorithm can noticeably improve the spatial resolution of reconstructed objects at high frame rates and sub-nm spectral resolution. Moreover, under different compression ratios, TVAL3 algorithm can not only reconstruct clear images, but also significantly improve the speed of reconstruction. In the process of reconstructing the spot motion, the motion trajectory of the spot reconstructed by the TVAL3 algorithm can well fit the fitting trajectory. Besides, due to the optical system, the collected light spot will be distorted, but the shape of the light spot reconstructed by the TVAL3 algorithm can be closer to the real light spot. Therefore, in the subsequent observation of the

Optical Materials EXPRESS

ultrafast process of unknown results, such as femtosecond laser direct writing, phase transition and laser filamentation, the reconstruction accuracy of the TVAL3 algorithm should be higher.

Funding. National Natural Science Foundation of China (12127806, 61875158, 62175195).

Acknowledgments. This work is supported by the National Science Foundation of China under the Grant nos. 12127806, 62175195, 61875158, the International Joint Research Laboratory for Micro/Nano Manufacturing and Measurement Technologies, the Fundamental Research Funds for the Central Universities.

Disclosures. The authors declare no conflicts of interest.

Data availability. Data underlying the results presented in this paper are not publicly available at this time but may be obtained from the authors upon reasonable request.

References

1. Z. Deng, F. Chen, Q. Yang, H. Bian, G. Du, J. Yong, C. Shan, and X. Hou, "Dragonfly-eye-inspired artificial compound eyes with sophisticated imaging," Adv. Funct. Mater. **26**(12), 1995–2001 (2016).
2. Y. Jia, R. He, Javier R Vázquez, V. de Aldana, H. Liu, and F. Chen, "Femtosecond laser direct writing of few-mode depressed-cladding waveguide lasers," Opt. Express **27**(21), 30941–30951 (2019).
3. S. Wang, X. Sun, H. Liu, Y. Ren, Y. Jia, and F. Chen, "Femtosecond laser direct writing of Nd:YLF cladding waveguides for efficient 1047-nm laser emission," Opt. Mater. Express **11**(9), 2915–2923 (2021).
4. A. Couairon and A. Mysyrowicz, "Femtosecond filamentation in transparent media," Phys. Rep. **441**(2-4), 47–189 (2007).
5. Q. Gong and W. Zhao, "Ultrafast science to capture ultrafast motions," Ultrafast Science **2021**, 1–2 (2021).
6. B. Guo, J. Sun, Y. Lu, and L. Jiang, "Ultrafast dynamics observation during femtosecond laser-material interaction," Int. J. Extrem. Manuf. **1**(3), 032004 (2019).
7. A. H. Zewail, "Laser femtochemistry," Science **242**(4886), 1645–1653 (1988).
8. S. Yeola, D. Kuk, and K.-Y. Kim, "Single-shot ultrafast imaging via spatiotemporal division of femtosecond laser pulses," J. Opt. Soc. Am. B **35**(11), 2822 (2018).
9. X. Wang, L. Yan, J. Si, S. Matsuo, H. Xu, and X. Hou, "High-frame-rate observation of single femtosecond laser pulse propagation in fused silica using an echelon and optical polarigraphy technique," Appl. Opt. **53**(36), 8395–8399 (2014).
10. K. Nakagawa, A. Iwasaki, Y. Oishi, R. Horisaki, A. Tsukamoto, A. Nakamura, K. Hirosawa, H. Liao, T. Ushida, K. Goda, F. Kannari, and I. Sakuma, "Sequentially timed all-optical mapping photography (STAMP)," Nat. Photonics **8**(9), 695–700 (2014).
11. T. Suzuki, F. Isa, L. Fujii, K. Hirosawa, K. Nakagawa, K. Goda, I. Sakuma, and F. Kannari, "Sequentially timed all-optical mapping photography (STAMP) utilizing spectral filtering," Opt. Express **23**(23), 30512–30522 (2015).
12. A. Ehn, J. Bood, Z. Li, E. Berrocal, M. Alden, and E. Kristensson, "FRAME: femtosecond videography for atomic and molecular dynamics," Light: Sci. Appl. **6**(9), e17045 (2017).
13. D. L. Donoho, "Compressed sensing," IEEE Trans. Inf. Theory **52**(4), 1289–1306 (2006).
14. L. Gao, J. Liang, C. Li, and L. V. Wang, "Single-shot compressed ultrafast photography at one hundred billion frames per second," Nature **516**(7529), 74–77 (2014).
15. Y. Lu, T. T. W. Wong, F. Chen, and L. Wang, "Compressed Ultrafast Spectral-Temporal Photography," Phys. Rev. Lett. **122**(19), 193904 (2019).
16. P. Wang, J. Liang, and L. V. Wang, "Single-shot ultrafast imaging attaining 70 trillion frames per second," Nat. Commun. **11**(1), 2091 (2020).
17. C. Yang, F. Cao, D. Qi, Y. He, P. Ding, J. Yao, T. Jia, Z. Sun, and S. Zhang, "Hyperspectrally Compressed Ultrafast Photography," Phys. Rev. Lett. **124**(2), 023902 (2020).
18. J. M. Bioucas-Dias and M. A. Figueiredo, "A new twIst: two-step iterative shrinkage/thresholding algorithms for image restoration," IEEE Trans. on Image Process. **16**(12), 2992–3004 (2007).
19. A. Chambolle, "An algorithm for total variation minimization and applications," J. Math. Imaging Vis. **20**(1/2), 73–87 (2004).
20. C. Li, W. Yin, H. Jiang, and Y. Zhang, "An efficient augmented Lagrangian method with applications to total variation minimization," Comput. Optim. Appl. **56**(3), 507–530 (2013).
21. Y. Wang, J. Yang, W. Yin, and Y. Zhang, "A new alternating minimization algorithm for total variation image reconstruction," SIAM J. Imaging Sci. **1**(3), 248–272 (2008).
22. C. Yang, D. Qi, F. Cao, Y. He, X. Wang, W. Wen, J. Tian, T. Jia, Z. Sun, and S. Zhang, "Improving the image reconstruction quality of compressed ultrafast photography via an augmented Lagrangian algorithm," J. Opt. **21**(3), 035703 (2019).
23. A. Wagadarikar, R. John, R. Willett, and D. Brady, "Single disperser design for coded aperture snapshot spectral imaging," Appl. Opt. **47**(10), B44–B51 (2008).
24. J. Park, D. J. Brady, G. Zheng, L. Tian, and L. Gao, "Review of bio-optical imaging systems with a high space-bandwidth product," Adv. Photon. **3**(04), 1044001 (2021).
25. L. Wang, P. Ho, C. Liu, G. Zhang, and R. Alfano, "Ballistic 2-D imaging through scattering walls using an ultrafast optical Kerr gate," Science **253**(5021), 769–771 (1991).